Atmos. Chem. Phys. Discuss., 11, 7423–7467, 2011
www.atmos-chem-phys-discuss.net/11/7423/2011/
doi:10.5194/acpd-11-7423-2011

Atmospheric Chemistry and Physics Discussions

Volatility and hygroscopicity of aging secondary organic aerosol in a smog chamber

T. Tritscher[1], J. Dommen[1], P. F. DeCarlo[1,*], P. B. Barmet[1], A. P. Praplan[1], E. Weingartner[1], M. Gysel[1], A. S. H. Prévôt[1], I. Riipinen[2,3], N. M. Donahue[3], and U. Baltensperger[1]

[1]Laboratory of Atmospheric Chemistry, Paul Scherrer Institut, Villigen, Switzerland
[2]Department of Physics, University of Helsinki, Helsinki, Finland
[3]Department of Chemical Engineering, Carnegie Mellon University, Pittsburgh, PA, USA
[*]now at: AAAS Science and Technology Policy Fellow Hosted at the US EPA, Washington, DC, USA

Received: 24 February 2011 – Accepted: 25 February 2011 – Published: 3 March 2011

Correspondence to: E. Weingartner (ernest.weingartner@psi.ch)

Published by Copernicus Publications on behalf of the European Geosciences Union.

Abstract

The evolution of secondary organic aerosols (SOA) during (photo-)chemical aging processes was investigated in a smog chamber. SOA from 10–40 ppb α-pinene was formed during ozonolysis followed by aging with OH radicals. The particles' volatility and hygroscopicity (expressed as volume fraction remaining (VFR) and hygroscopicity parameter κ) were measured with a volatility and hygroscopicity tandem differential mobility analyzer (V/H-TDMA). These measurements were used as sensitive physical parameters to reveal the possible mechanisms responsible for the chemical changes in the SOA composition during aging: A change of VFR and/or κ during processing of atmospheric aerosol may occur either by addition of SOA mass (by condensation) or by an exchange of molecules in the SOA by other molecules with different properties. The former process increases the SOA mass by definition, while the latter keeps the SOA mass roughly constant and may occur either by heterogeneous reactions on the surface of the SOA particles, by homogeneous reactions like oligomerization or by an evaporation – gas-phase oxidation – recondensation cycle. Thus, when there is a substantial change in the aerosol mass with time, the condensation mechanism may be assumed to be dominant, while, when the mass stays roughly constant the exchange mechanism is likely to be dominant, a process termed ripening here. Depending on the phase of the experiment, an O_3 mediated condensation, O_3 mediated ripening, OH mediated condensation, and OH mediated ripening could be distinguished.

During the O_3 mediated condensation the particles volatility decreased (increasing VFR) while the hygroscopicity increased. Thereafter, in the course of O_3 mediated ripening volatility continued to decrease, but hygroscopicity stayed roughly constant. After exposing the SOA to OH radicals an OH mediated condensation started with a significant increase of SOA mass. Concurrently, hygroscopicity and volatility increased. This phase was then followed by an OH mediated ripening with a decrease of volatility.

ACPD

11, 7423–7467, 2011

1 Introduction

Secondary organic aerosols (SOA) are a major constituent of the atmospheric particulate matter and originate from chemical transformation of primary volatile organic compounds (VOC) to lower volatility products that partition into the condensed phase. Many studies have already been performed on SOA formation and properties (see e.g. references in Hallquist et al. 2009). One of the major challenges for SOA studies is the multi-component composition of SOA with only few known substances among thousands of unknown species. Field measurements show changing SOA properties with oxidative aging, but detailed studies of these processes under ambient conditions in the lab are challenging and thus scarce (Rudich et al., 2007).

It is challenging for the state-of-the-art chemical transport models to reproduce the measured ambient organic aerosol concentrations (i.e. directly emitted primary organic aerosol (POA) and SOA formed from various precursors) with currently known chemical and physical mechanisms (Volkamer et al., 2006; Hodzic et al., 2010). One important challenge in modeling SOA mass in the atmosphere or under laboratory conditions is the correct implementation of the gas-particle interactions such as the partitioning effect Pankow (1994a,b). The semi-volatile nature of the SOA particles including their gas-particle partitioning behavior was recently described by the volatility basis set (VBS) approach (Donahue et al., 2006; Robinson et al., 2007; Jimenez et al., 2009), which lumps the various organic compounds together according to their effective saturation mass concentration (C^*). This is the mass equivalent of the saturation vapor pressure, which controls volatility. Volatility is a key property of the organic components of the gas and particulate phase and it determines the SOA formation and the partitioning between the phases.

Laboratory experiments e.g. in chambers span a wide range of semi-volatile oxygenated organic aerosol (SV-OOA), but low-volatility oxygenated organic aerosol (LV-OOA), as found in ambient measurements of aged air masses, is still difficult to study and reproduce under laboratory conditions (Jimenez et al., 2009). The atomic oxygen

ACPD
11, 7423–7467, 2011

to carbon ratio (O:C ratio) of SOA can be used to roughly split the mass to SV-OOA and LV-OOA components. It also allows the classification of organics within the VBS framework.

Formation of SOA involves at least three main types of chemical transformation: oligomerization, functionalization and fragmentation (Jimenez et al., 2009). During oxidation processes functionalization and fragmentation occur, driving an increase in the O:C ratio. Volatility decreases during functionalization and (mostly) increases during fragmentation as molecules become smaller. Oligomerization is a chemical process that converts monomers to larger, less volatile compounds (Kalberer et al., 2004). During oligomerization the volatility decreases while the O:C ratio may be increased or reduced, depending on the process (Reinhardt et al., 2007; Jimenez et al., 2009). The expected behavior of the volatility during the three main processes is summarized in Table 1.

Aerosols, including SOA but also inorganic and other organic substances, have an influence on global climate via the direct aerosol effect by scattering sunlight and via the indirect aerosol effect by changing cloud properties and characteristics (Lohmann and Feichter, 2005). Hygroscopicity, the degree of water uptake by particles, is an important parameter for both effects and has been studied for different SOA types e.g. (Baltensperger et al., 2005; Varutbangkul et al., 2006; Prenni et al., 2007; Duplissy et al., 2008; Juranyi et al., 2009; Qi et al., 2010). A positive correlation between hygroscopicity and O:C ratio has been shown recently (Jimenez et al., 2009; Chang et al., 2010; Massoli et al., 2010; Duplissy et al., 2011). The following equation for the hygroscopicity parameter κ can be derived from Petters and Kreidenweis (2007) to represent the hygroscopicity of an aerosol:

$$\kappa = v_w \times \frac{\rho_s}{M_s} \times i_s, \quad (1)$$

where v_w is the partial molar volume of water, M_s, ρ_s and i_s the molar mass, density and effective van't Hoff factor of the solute. v_w is in good approximation constant across

ACPD
11, 7423–7467, 2011

the water activity range of interest. This leaves i_s and ρ_s/M_s as the two key factors determining particle hygroscopicity (κ). The expected effect of the three main chemical processes on i_s and ρ_s/M_s and thus κ is summarized in Table 1. Functionalization typically increases i_s due to positive interactions between polar functional groups and water (Petters et al., 2009). Additional dissociation effects would also increase i_s, though the degree of dissociation of carboxyl and hydroxyl groups is likely very small. Only a small increase, if at all, is expected for M_s and ρ_s, and thus changes of ρ_s/M_s will be small. κ is thus expected to increase under the influence of functionalization. Oligomerization strongly increases M_s with little effect on ρ_s, resulting in a decrease of ρ_s/M_s. Only small changes are expected for i_s. Overall a decrease of κ is expected under the influence of oligomerization, though the effect becomes smaller with increasing M_s (Petters et al., 2006). Opposite effects are essentially expected for fragmentation compared to oligomerization. Equation 1 describes the hygroscopicity of completely dissolved solutes. Particle hygroscopicity would be reduced if the SOA was only partially soluble. Functionalization increases the solubility, while oligomerization and fragmentation are expected to have little effect on the solubility. The qualitative overall effects of the three main chemical reactions on aerosol hygroscopicity as described in Table 1 remain thus also valid if additional effects of limited solubility occur. In general the number of species (molecules or ions) going into solution matters for the hygroscopicity, this can be expressed as the van't Hoff factor. Highly oxidized organic molecules like acids can dissociate in water and have thus a higher hygroscopicity than a hydrocarbon with little functional groups.

The chemical and physical characterization of SOA is often discussed separately (Hallquist et al., 2009). So far it is not clear how oxidation (aging) changes the amount and properties of SOA. Here we investigate the aerosol physical properties of SOA volatility and hygroscopicity as a function of the oxidant exposure under controlled conditions. Comparing trends of volatility and hygroscopicity may shed light on the dominant processes (functionalization, condensation and oligomerization) under the influence of different aging processes. These measurements were conducted at the

ACPD
11, 7423–7467, 2011

Paul Scherrer Institut (PSI) smog chamber within the scope of the MUCHACHAS (Multiple Chamber Aerosol Chemistry and Aging Studies) campaigns. MUCHACHAS took place in several chambers in Europe and the US with different points of emphasis for a similar set of experiments. The main emphasis for the MUCHACHAS experiments at the PSI smog chamber was the aging of α-pinene (AP) SOA with OH under dark and light conditions.

2 The experimental setup

2.1 Smog chamber and associated instruments

The air in the 27-m^3 Teflon bag in a temperature controlled chamber with four filtered xenon lamps providing quasi-solar illumination is monitored by several gas and aerosol phase instruments described in detail in Paulsen et al. (2005). Here we mention the main instruments relevant for this paper and the experimental procedure. The particles volatility and hygroscopicity were characterized with a volatility and hygroscopicity tandem differential mobility analyzer (V/H-TDMA, see Sect. 2.2). The aerosol particle number size distribution (diameter $D = 20 - 800$ nm) and chemical composition were measured with an scanning mobility particle sizer (SMPS) and an Aerodyne high resolution time of flight aerosol mass spectrometer (AMS). The AMS detects inorganic and organic aerosol species quantitatively and is described elsewhere in detail (DeCarlo et al., 2006). It allows the chemical quantification and characterization of several types of fragments of the SOA with a time resolution of minutes (e.g. Alfarra et al. 2006). The organic aerosol mass measurement from the AMS was wall-loss corrected to account for the losses to the chamber walls. Assuming that the wall loss rate is first order and independent of size we used an exponential fit asymptotically decreasing to 0 to correct for the losses (Pathak et al., 2007). In the following the terms "organic aerosol mass" or "SOA mass" always relate to wall-loss corrected organic particulate mass. A very useful parameter derived from AMS data is the oxygen to carbon ratio (O:C ratio)

ACPD
11, 7423–7467, 2011

(Aiken et al., 2007, 2008), which is linked to the hygroscopicity properties of the aerosol (Duplissy et al., 2011).

The gas-phase instruments include NO_x monitors (Monitor Labs 9841A, Thermo Environmental Instruments 42C) and ozone monitors (Monitor Labs 8810, Environics S300). A proton transfer reaction mass spectrometer (PTR-MS) from IONICON was deployed as well. The high sensitivity PTR-MS (Lindinger et al., 1998) is able to detect VOCs in real-time with a very low detection limit (ppt level). From the measurement of the precursor α-pinene we calculated "AP reacted". However, after injection of AP into the ozone (O_3) containing chamber the initial concentration was not directly measured because AP needs to mix first and already starts to react with O_3. It was therefore determined from fitting the AP concentration back to the injection time.

2.2 V/H-TDMA instrument

We built a new V/H-TDMA instrument which is described and characterized in more detail here. The tandem differential mobility analyzer (TDMA) technique (Rader and McMurry, 1986) is a common technique to characterize aerosol properties. The H-TDMA technique is well established and a suitable method to measure the hygroscopicity of submicrometer aerosol (Swietlicki et al., 2008). Our combined volatility and hygroscopicity tandem differential mobility analyzer (V/H-TDMA) runs volatility and hygroscopicity scans in parallel (Fig. 1). The aerosol is conditioned before entering the first differential mobility analyzer (DMA1) by passing through a diffusion dryer and a Kr-85 bipolar charger to bring the particles into charge equilibrium. All DMAs are situated in a temperature controlled, well insulated housing at 20 °C. DMA1 size selects a dry (RH<15%), quasi-monodisperse aerosol, which is split into a heater and a humidifier flow (0.3 L/min each). Two additional DMAs scan the heated or humidified particles (DMA2 and DMA3, respectively) which are then counted with the condensation particle counter for hygroscopicity (CPC_H) and the CPC_V (CPC for volatility), respectively.

The H-TDMA part is based on the design of a previous instrument (Duplissy et al., 2008, 2009). The individual sheath air flows are operated in closed loops and the

ACPD
11, 7423–7467, 2011

flows are maintained with blowers (Fig. 1), which is controlled by laminar flow elements combined with differential pressure sensors and proportional-integral-derivative (PID) controllers. A separate humidifier loop with bubbler (not shown in Fig. 1) supplies the humidifier with humid air. The humidifier section is situated in a second, temperature controlled housing at 24 °C. The aerosol can be humidified up to a controlled relative humidity (RH) of 97±1% with a residence time of ~26 s (between DMA1 and DMA2).

Measurement of the deliquescence RH of ammonium sulfate (AS) and other salts e.g. sodium chloride (NaCl) are used for the calibration of the dew point mirror (see Fig. 1) to assure accurate RH measurement. The correct absolute sizing of the DMAs is periodically checked with polystyrene latex spheres (PSLs) having dry diameters D_0 between 100 and 350 nm. The correct sizing of the DMAs with respect to each other is frequently checked by conducting a series of measurements without heating and humidifying. This relative calibration of DMA1 with DMA2 /DMA3 is important to detect small instrumental drifts which would affect the precision of the growth factor measurements (the error in D/D_0 is typically <1%).

The heater in the V-TDMA part is custom-built and consists of an inner linear brass tube (70×2.2 cm) surrounded by capillary tubes containing a heating wire. The small space between these capillary tubes allows for a rapid cooling with pressurized air. The temperature sensor in the center of the inner tube (see Fig. 1) controls the heater temperature (T) in a range from 25–200 °C (±2 °C). Modeling of the temperatures and flow streamlines inside the heater suggests a laminar flow and a homogeneous temperature distribution after at most 15 cm from the inlet. The calculated plug flow residence time (RT) in the heater for 25–200 °C is 24.4–15.4 s at a constant aerosol flow of 0.6 L/min. The aerosol flow is diluted with filtered, pure air before (0.3 L/min) and after the heater (0.4 L/min) to maintain correct aerosol flows in all parts of the instrument. Measurements of the aerosol particles' average "traveling time" from the outlet of DMA1 to the inlet of DMA3 (including heater and tubing) was found to be 23±2 s at 30 °C. The RT is longer compared to other heaters employed in TDMAs (Paulsen et al., 2005; Jonsson et al., 2007; Villani et al., 2007) and thermodenuder

ACPD
11, 7423–7467, 2011

(Burtscher et al., 2001; Wehner et al., 2002). This typically results in a lower remaining aerosol volume at a specific temperature (An et al., 2007). As particle concentrations are rather small, a denuder is not needed in our system because the inner surface of the heater offers much larger surface for the vapors to condense than the aerosols. Nucleation, an indicator for re-condensation of vapors, was not observed in the V-TDMA.

In general the parameters obtained from the TDMA are the growth factor GF(RH), and shrinking factor SF(T) defined as the ratio of humidified diameter D(RH), or heated diameter $D(T)$ and initial dry and non-heated diameter (D_0), respectively:

$$\mathrm{GF(RH)} = \frac{D(\mathrm{RH})}{D_0} \quad (2)$$

$$\mathrm{SF}(T) = \frac{D(T)}{D_0} \quad (3)$$

The raw growth or shrinking factor distributions measured by the V- and H-part are analyzed using the TDMAinv approach (Gysel et al., 2009) in order to obtain inverted and calibrated probability density functions (PDF). Details on this data analysis procedure and especially on the used TDMAinv approach are found in Gysel et al. (2009). In the following the hygroscopic growth factor (GF) always refers to the number weighted mean GF (1st moment) of the inverted GF-PDF, and the shrinking factor (SF) to the volume weighted mean SF (3rd moment) of the inverted SF-PDF. Instead of SF the volume fraction remaining (VFR), defined as $\mathrm{VFR} = \mathrm{SF}^3$, is chosen to present the volatility data.

In this study the H-TDMA was typically operated at a constant high RH of 95%. The RH was very stable, and the GF data in the RH range 93–97% were corrected to 95.0% RH in order to exclude any uncertainties caused by this small variation (Gysel et al., 2009). The V-TDMA heater was running mainly at 70 °C (with a plug flow RT of 21 s) and only data in the range T = 68–72 °C were considered in the analysis. We minimize chemical perturbations of the composition (pyrolysis) in the heater with this relatively

ACPD
11, 7423–7467, 2011

low thermodenuder temperature. During few experiments the heater temperature was varied (from 25 to 200 °C) to measure the VFR as a function of temperature, resulting in a thermogram plot.

The measured D_0 are in the total range from 50 to 250 nm, where low AP experiments range from 50 to 150 nm and high AP precursor concentrations range from 75 to 250 nm. D_0 was chosen for several diameters with long overlapping time. D_0 had to be changed if the number size distribution in the smog chamber changed in a way that the D_0 of the V/H-TDMA was out of the range or had too few counts. Typically particles are small in the beginning of an SOA experiment, but grow very rapidly during the ozonolysis and stabilize at a diameter of a few hundred nanometers. We present the hygroscopicity results mainly in the single hygroscopicity parameter κ (see also equation 1, Petters and Kreidenweis 2007) to account for the size dependence of the GF (Kelvin effect). κ was calculated assuming the surface tension of pure water. A κ of 0 corresponds to GF = 1. The use of κ allows for direct comparison with other studies or measurements e.g. from a cloud condensation nucleus counter.

The V-TDMA was characterized with laboratory generated particles of known chemical composition to allow for a comparison of the results with other systems. The instrument residence time, diameter, and concentration of aerosols are important factors for heater characterization. Figure 2 shows the VFR for different compounds and particle diameters as function of the heater temperature.

Panel A in Fig. 2 displays the VFR of NaCl, which is known to be non-volatile up to temperatures clearly above 200 °C (Scheibel and Porstendoerfer, 1983), and thus the VFR measured by the V-TDMA is expected to be unity across the whole temperature range. The very small observed decrease in VFR to ~0.97 at 200 °C might be either a restructuring/reorientation effect, which would result in a more compact structure and therefore smaller effective volume, or evaporation of impurities from the nebulizing process of NaCl. A similarly stable volatility behavior is observed in other studies (e.g. Modini et al. 2010). The plot of NaCl shows also the high precision of the instrument with less than ±2% for VFR. Thermophoretical losses at 200 °C were determined

ACPD
11, 7423–7467, 2011

to be 10–15% in particle number for NaCl particles with D_0 = 35–200 nm. This is in the range of other thermodenuders (Huffman et al., 2008; Park et al., 2008). We consider the losses as less relevant because the instrument is not quantitative in particle mass or number but rather measures the physical properties volatility and hygroscopicity.

Citric acid (Fig. 2B) was chosen as a reference substance because it is of rather high volatility similar to SOA; VFR starts to decrease at $T > 70\,^{\circ}C$. At temperatures above 110 °C particles with $D_0 \leq 300$ nm are completely evaporated in our instrument. A small size-dependence due to kinetic reasons is seen: smaller particles tend to evaporate faster than larger particles (see e.g. Riipinen et al. 2010).

Ammonium sulfate particles (AS) (Fig. 2C) are often used for heater characterization; in our system AS particles start to volatilize at temperatures $T > \sim 100\,^{\circ}C$. All AS particles volatilize completely (i.e. VFR < 0.15) at temperatures above 150 °C. Compared to literature data the thermogram of the mass fraction remaining from AMS for polydisperse AS in Wu et al. (2009) looks similar as ours, with a rapid decrease of the mass fraction remaining between 120 °C and 160 °C. Villani et al. (2007) present an overview table with 160 - 180 °C at D_0 = 15–150 nm as lowest volatilization temperature for AS in their V-TDMA instrument while other studies report even higher temperatures. There are also studies where AS starts to volatilize around 110 °C, but does not evaporate completely even at temperatures above 230 °C (Huffman et al., 2008). In contrast to other studies and our V-TDMA there is a thermodenuder study where the diameter of AS decreases at lower temperatures around 75 °C, but 150 °C is needed to volatilize the particles completely (D_0 = 100 and 200 nm) (An et al., 2007).

Overall our instrument seems to be in a good temperature and residence time range for volatilization measurements of AS. Nevertheless, organic substances (e.g. citric acid) with relatively high volatility might be better suited to characterize a thermodenuder system than salts like AS because they often evaporate already at lower temperatures, i.e., more gentle heating is needed.

ACPD
11, 7423–7467, 2011

2.3 Smog chamber operation

The typical design of the MUCHACHAS experiments is shown as schematic in Fig. 3. The precursor in all experiments described here was α-pinene (AP). The concept was to first form SOA from ozonolysis, allow it to stabilize after nearly all the precursor was consumed, and then to expose the first-generation SOA and partially oxidized gas-phase species to OH radicals in order to observe changes caused by OH aging.

A change of the VFR and/or the κ value during processing of atmospheric aerosol may occur either by addition of SOA mass (by condensation) or by an exchange of molecules in the SOA by other molecules with different properties. The former process increases the SOA mass by definition, while the latter keeps the SOA mass roughly constant and may occur either by heterogeneous reactions on the surface of the SOA particles or by evaporation – gas-phase oxidation – recondensation cycle. Thus, when there is a substantial change in the aerosol mass with time, the condensation mechanism may be assumed to be dominant, while, when the mass stays roughly constant the exchange mechanism is the likely dominant process. In our experiments both mechanisms may be mediated by either ozone or OH radicals. In the light of this, we assign the following four dominating mechanisms to four different phases of our experiments (see Fig. 3): O_3 mediated condensation, O_3 mediated ripening, OH mediated condensation, and OH mediated ripening. In the condensation phases, the physical (VFR, κ) and chemical (O:C ratio) properties are believed to mainly vary as a result of the additional condensing material, while ripening refers to chemical transformation of the SOA without significant change of the mass.

In all experiments, the clean smog chamber was humidified to ~50% RH and in a first step O_3 was added. After about 20 min when the O_3 was distributed homogeneously in the bag the precursor AP was injected. We conducted experiments at two atmospherically relevant precursor concentrations of 40 ppb ("high") and 10 ppb ("low") α-pinene concentration. The reaction started immediately forming particles (first-generation SOA) from the ozonolysis of the C=C double bond in AP. The OH

ACPD
11, 7423–7467, 2011

formed by the ozonolysis will mainly react with the AP, as long as this is still present in excess. Ozonolysis lasted a few hours until at least 90% of the AP precursor had reacted (Fig. 3).

In a next step, 20 ppb of 3-pentanol was added. Pentanol reacts with OH only, and thus its decay can be used as an OH tracer, in the same way as specific intermediate products. SOA was exposed to OH aging by either photolysis of HONO ("HONO photolysis experiments") or ozonolysis of tetramethylethylene (TME) (IUPAC name: 2,3−dimethyl−2−butene) ("dark OH (TME) experiments") (Epstein and Donahue, 2008). A list with details of all conducted experiments is given in Table 2.

A HONO level of 15-20 ppb (as measured by a Long Path Absorption Photometer (LOPAP)) in the chamber was reached by passing pure air (2 L/min) through a custom built vessel with sulfuric acid (0.01 M H_2SO_4) and sodium nitrite (3×10^{-3} M $NaNO_2$). The vessel and the HONO system are described elsewhere (Taira and Kanda, 1990). The flow from the HONO generator was passed through a filter to ensure that only the gas phase HONO without particles entered into the chamber. The addition of HONO started about one hour before the lights were turned on. In some high-NO_x photolysis experiments (Table 2, exp. No. 6–8) 50–80 ppb NO was added in addition to the HONO. TME was continuously injected from a gas cylinder (Messer, TME 1000 mol ppm in N_2 5.0) at a flow of 10 mL/min. The ozone level was usually higher in the TME experiments compared to HONO photolysis experiments because O_3 was also needed for the ozonolysis of TME.

Different time axes as shown in the concept figure (Fig. 3) are used in the following. Two "physical time" clocks (in units of hour (h) are used; one is related first to the "time after AP injection" which is the time of the start of the ozonolysis reaction. The second time axis is "time after OH started" indicating the start of the OH aging, which can be either the time when the lights were turned on or when the continuous injection of TME started. Two "chemical time" clocks are used to represent the experiments with respect to their experienced reaction dependence on the concentration of the respective reactants. The O_3 exposure integrated over time (in h ppb) serves as chemical

ACPD
11, 7423–7467, 2011

time during the ozonolysis, and the integrated OH exposure time (in $h\,cm^{-3}$) is used during the reaction period with OH. The OH concentration was calculated from the decay rate of pinonaldehyde as measured by PTR-MS (see Barmet et al., in preparation). Pinonaldehyde is a reaction product of AP ozonolysis. OH concentrations in the experiments were between 2×10^6 and 10^7 molecules per cm^3. Due to the fast reaction of pinonaldehyde with OH the OH exposure time was limited to about $15\times10^6\,h\,cm^{-3}$.

3 Results and discussion

First we present thermograms (temperature ramping in the V-TDMA heater) of some SOA experiments for comparison with reference substances (Sect. 2.2) and with other studies (Sect. 3.1). However, the main focus in this paper is on the temporal evolution of κ (GF) and VFR during the ozonolysis (Sect. 3.2) and the OH exposure phases (Sect. 3.3). Thus time series at constant heater temperature ($T = 70\,^{\circ}C$) in the V-TDMA and relative humidity ($RH = 95\%$) in the H-TDMA allow for a closer look at the ongoing processes during different reaction periods, mechanisms and conditions (see Sect. 2.3). Finally, the correlation of VFR and κ (Sect. 3.4) will be investigated as well as the effect of additional light and the size dependence (Sect. 3.5) of these measured properties.

3.1 Thermogram of SOA and comparison with other studies

Thermograms with well known substances characterize the V-TDMA (Fig. 2) as discussed above. Such thermal information can also be used to gain information on the complex chemical nature of SOA. Figure 4 shows mean VFR values versus heater temperature for all three types of AP SOA experiments (circles). Four thermograms from other studies of AP SOA (squares) are compared to our measurements. The error bars represent the standard deviations of VFR (vertical) and the temperature (horizontal). Large vertical error bars are due to real volatility changes of the chamber

ACPD
11, 7423–7467, 2011

aerosol during the course of the experiment and do not reflect the V-TDMA accuracy. All our thermograms are similar within these uncertainties and show no distinct D_0 or experiment type dependence.

A significant decrease of VFR starts at ~50 °C and by 90 °C 50% of the particle volume is volatilized. Temperatures around 150 °C are required to reduce the VFR to 10%. This is a much wider temperature range than for pure citric acid or ammonium sulfate and is explained with different compounds in the chamber SOA possessing volatilities ranging from rather semi-volatile to low-volatile. The SOA produced purely by ozonolysis tends to be slightly more volatile than after aging with OH. The three experiment types (ozonolysis, HONO photolysis and dark OH (TME) experiments) cannot be compared in detail as they comprise different temperature setting and reaction times. Nevertheless, our thermograms were fitted with an error function (erf) (Fig. 4, black line, only valid above 50 °C); it is set to 1 as maximum and has the following equation with T as the heater temperature:

$$\mathrm{VFR} = 0.91 - 0.911 \times \mathrm{erf}\left(\frac{T[^{\circ}\mathrm{C}] - 53.15}{82.5}\right) \quad (4)$$

This fit is helpful to extrapolate the volatility data from other experiments during this study when the temperature was set to 70 °C continuously to compare e.g. with other studies. Comparison of our measurements with other AP SOA studies (squares in Fig. 4) shows the best agreement with the instrument and measurements from Jonsson et al. (2007) for low temperatures and Huffman et al. (2009) for higher temperatures. Our SOA thermograms lie between the two other studies from An et al. (2007) and Paulsen et al. (2005). Different residence times (RT) in the heated zone are an important reason for the encountered differences in the thermograms. The plug flow RT from the other studies are <1 s (Baltensperger et al., 2005; Paulsen et al., 2005), 2.8 s (Jonsson et al., 2007), 21.2 s (Huffman et al., 2008, 2009) and 31.6 s (An et al., 2007), respectively. If the above papers stated the centerline RT at laminar flow we converted it to plug flow RT (factor 2). Our instrument seems to have the second longest RT, ca.

ACPD
11, 7423–7467, 2011

23 s at ambient temperature (see Sect. 2.2); only the RT from An et al. (2007) is longer. This could explain the stronger volatilization of SOA at relatively low temperatures in their study at least partly. On the other hand shorter RT leads to higher VFR (Baltensperger et al., 2005; Paulsen et al., 2005; Jonsson et al., 2007). Other factors like initial particle size, monodisperse or polydisperse measurement, or the use of a charcoal denuder after the heating section may also be responsible for some differences between the various studies. With our long RT we are able to use low temperatures in the heater and minimize kinetic limitations of evaporation and hope to be close to equilibrium, even though this might be not the case as suggested recently (Riipinen et al., 2010). Further reasons for small differences in the SOA thermograms may be the type AP SOA, its concentration, and experimental conditions.

Overall, the comparison of thermograms gives an orientation on our V-TDMA characteristics and shows the importance of the residence time. The decrease in VFR with temperature is experienced over a relatively large temperature range and offers a sensitive range from ~60 to 100 °C to study the SOA volatile properties. In the following discussion a constant oven temperature of 70 °C was chosen to track temporal changes in the SOA volatility during the chamber reactions.

3.2 Ozonolysis – O_3 mediated condensation and ripening

The first step in each experiment was the ozonolysis of AP to form SOA mass (Fig. 3). The initial O_3 concentration varied with the type of experiment. Figure 5 shows the time trends of the fraction of AP reacted, the organic aerosol mass, the volatility as VFR, and the hygroscopicity both as κ value and as GF at 95% RH. The markers are colored according to the initial O_3 concentration (blue = low O_3 and orange = high O_3 concentration); filled symbols represent low AP and open symbols represent high AP input.

High O_3 concentrations led to a fast reaction of AP and a rapid formation of SOA (Fig. 5, panel A-B). It took roughly one hour to reach the "90% AP reacted" level (see vertical lines in Fig. 5). At lower O_3 concentrations this took 2–3 times longer and the

ACPD
11, 7423–7467, 2011

final SOA mass was lower. This may have two reasons. Firstly, more semi-volatile compounds are lost to the walls and do not condense on the particles. Secondly, organic radical-radical reactions are decreased, eventually leading to less semi-volatile compounds contributing to SOA.

The physical parameters κ and VFR data (Fig. 5, panel C-D) split mainly into two groups comprising low and high concentration AP experiments. Experiments with high SOA mass have generally a higher volatility (lower VFR) and lower hygroscopicity. In case of the low AP experiments VFR increases steadily from 0.55 to 0.7 after 4.5 h of reaction. Even after most of the AP had reacted (90%-level) VFR keeps increasing. The high AP experiments show a similar but less pronounced trend. During the condensation phase VFR slightly increases. The split into low and high AP experiments is less clear for the hygroscopicity in the very beginning; they separate more with time (Fig. 5D, E). Other studies found a distinct mass concentration dependence of GF (Duplissy et al., 2008). During the ozonolysis and the beginning of the OH mediated condensation phase this is not the case for all experiments, but Duplissy et al. (2008) had higher AP concentrations (>120 ppb) in their study and investigated a different system (photolysis instead of pure ozonolysis), which can explain the differences in the findings.

The hygroscopicity is presented in Fig. 5 (panel D-E) in terms of κ and GF to allow a direct comparison. Both show the same features (small difference between high and low AP experiments) and differences between κ and GF are mainly seen during the first 1–2 h of ozonolysis where the selected diameters are small and differ due to fast particle formation. In some experiments (open blue circle at about 5 h, two diameters are measured alternately) the GF seems to smooth size effects of different diameters. The presented κ values are a good proxy for the particles' hygroscopicity because the diameter dependence of the Kelvin effect is taken into account (by assuming a surface tension of pure water). Thus we will present the hygroscopicity data as κ values in the following. The κ values start at about 0.04 in the beginning of all experiments and then increase during the condensation phase. Thereafter, κ remains almost constant.

ACPD
11, 7423–7467, 2011

Similar as for VFR, the low AP concentration experiments group together and show a higher κ than the high AP concentration experiments. However, the values remain within a rather narrow range of 0.08–0.12.

Plotting κ and VFR versus the integrated O_3 exposure time (in h ppb) (Fig. A) splits the data into low and high O_3 concentration experiments. Figure A shows exactly the same experiments and parameters (panel A-D) as Fig. 5 with addition of the O_3 concentration (panel E) on a chemical time clock axis. Thus experiments are stretched or compressed compared to the physical time clock (in Fig. 5). The increase of κ and VFR during the O_3 mediated condensation and the rather constant values during the O_3 mediated ripening are again visible. The dose of O_3 is important; it determines the initial situation of the following OH reactions.

3.3 SOA aging – OH mediated condensation and ripening

During the first phase of the experiment the ozonolysis removed the precursor and formed a certain mass of SOA and first generation gaseous oxidation products. We then turned on an OH-radical source and monitored any changes in the amount and properties of SOA. Figure 6 shows the organic aerosol mass (panel A), the VFR at 70 °C (panel B), as well as κ and O:C ratio (panel C) for a low (green) and a high (blue) AP concentration using HONO photolysis as OH radical source. The time axis is given as "time after lights on" (TALO), which means that negative values denote the previous ozonolysis phase. Immediately after the onset of the OH radical source additional SOA mass is formed. Figure 6a shows that after correction for wall loss the SOA mass increases by 40–100%. This is a lower limit as the wall loss correction presented here is conservative – the effects of aging on SOA levels will be discussed in detail in a separate publication. We divide the OH mediated oxidation phase into an OH mediated condensation phase (TALO ~0 to 2 h), and OH mediated ripening (TALO ~2 to 4.5 h).

The hygroscopicity parameter κ (Fig. 6C) increases slightly during the OH mediated condensation phase and then stays constant during the OH mediated ripening. Hy-

ACPD
11, 7423–7467, 2011

groscopicity is not affected abruptly by the addition of new mass after OH exposure starts. This suggests similar hygroscopic properties of the new condensing material compared to the existing particle phase material. The O:C ratio is constant or slightly decreasing during the O_3 mediated phase, while it correlates well with κ during the OH mediated phase. Contrary to this the VFR (Fig. 6B) abruptly decreases after OH aging commences (turning lights on) and starts to stabilize after about one hour of aging with OH radicals. During the OH mediated ripening the VFR tends to increase slightly. The newly added organic aerosol mass after the onset of OH oxidation seems to have a higher volatility (lower VFR) than the existing organic aerosol. For example, the Zdanovskii-Stokes-Robinson equation (ZSR) (Stokes and Robinson, 1966) is used to predict from pure compound properties the hygroscopicity of mixed particles e.g. (Choi and Chan, 2002; Gysel et al., 2007; Moore and Raymond, 2008; Sjogren et al., 2008). The ZSR approximation assumes independent volatility behavior of the individual fractions in the mixed particle. Here we use this mixing rule as a two-component model to calculate the volatility of the newly added organic aerosol mass with the following equation:

$$\mathrm{VFR} = \mathrm{VFR}_{\mathrm{old}} \times \epsilon_{\mathrm{old}} + \mathrm{VFR}_{\mathrm{new}} \times (1 - \epsilon_{\mathrm{old}}) \quad (5)$$

$$\mathrm{VFR}_{\mathrm{new}} = \frac{\mathrm{VFR} - \mathrm{VFR}_{\mathrm{old}} \times \epsilon_{\mathrm{old}}}{1 - \epsilon_{\mathrm{old}}} \quad (6)$$

where $\mathrm{VFR}_{\mathrm{new}}$ is the calculated volume fraction remaining of the newly added SOA mass and VFR is measured with the V-TDMA. The volume fractions ϵ are derived from the organic aerosol mass measurements by the AMS before (ϵ_{old}) and after (1-ϵ_{old}) new material was added, assuming the same density for old and new mass. $\mathrm{VFR}_{\mathrm{old}}$ is the volume fraction remaining obtained by extrapolating a linear fit through the last 3 hours of ozonolysis. The resulting linear regression lines for the low AP experiment (No. 4) and for the high AP experiment (No. 7) are given in the figure.

Using the $\mathrm{VFR}_{\mathrm{old}}$ after one hour of exposure to OH, the newly condensed material has a calculated $\mathrm{VFR}_{\mathrm{new}}$ of 0.24 and 0.04 for the low and high precursor experiment,

ACPD
11, 7423–7467, 2011

respectively. The results are very similar if we assume a constant VFR (0.72, 0.69) at 70 °C for the initial aerosol before "lights on" (TALO = 0) instead of the VFR_{old}. This calculation shows that the freshly added material is highly volatile. We hypothesize that the SOA formed after OH exposure consists of smaller molecules with slightly higher O:C atomic ratios than the original SOA, which condenses onto the particles during this phase of the experiment.

In Fig. 7 all experiments are summarized. Panels A and B group the experiments according to the type of OH radical source (HONO photolysis and dark OH (TME)) while panels C and D show the dependence of κ and VFR on the wall-loss corrected SOA mass. OH exposure integrated over time is used as a chemical clock to bring all experiments on a comparable time scale. Some experiments are not shown in their full experimental length because this chemical OH clock is limited in time to when the pinonaldehyde concentration was high enough to be measured by the PTR-MS with high signal to noise ratio (see Sect. 2.3).

Overall, the time trends of κ and VFR (Fig. 7, panel A/B) are similar for all experiments and to those discussed above for the two experiments shown in Fig. 6. The initial values of κ and VFR are somewhat variable, depending on the preparation of the SOA by ozonolysis as discussed in Section 3.2. The κ values start at 0.07–0.12 and increase to 0.10–0.15 during the OH mediated condensation. The addition of new aerosol mass increases hygroscopicity, which indicates that the new mass is more hygroscopic than the original aerosol mass. During the second phase, the OH mediated ripening κ increases just slightly but stays almost constant. A linear regression over the whole OH mediated phase results in a mean straight line of $\kappa = 0.00137\ t + 0.105$ ($R^2 = 0.46$).

The VFR decreases during the OH mediated condensation and increases during the OH mediated ripening after about 8×10^6 h cm^{-3} OH exposure. The high concentration dark OH (TME) experiment No. 11 is the exception – VFR increases during both phases as it is the experiment with the highest organic aerosol mass. The type of OH source, dark OH (TME) and HONO photolysis does not show differences in the

ACPD
11, 7423–7467, 2011

particles' hygroscopicity or volatility behavior. This also indicates that high or low NO_x conditions during HONO photolysis experiments have no clear influence on κ and VFR (see Table 2).

In panel C and D (Fig. 7) the κ and VFR data of each experiment are colored by the SOA mass concentration measured by the AMS. The volatility of the high mass experiments is generally higher (lower VFR) than for the low AP experiments throughout the experiment. The spread of VFR becomes narrower with time. At the end of the OH mediated ripening phase κ values are lower for high AP experiments compared to the low concentration ones.

3.4 Correlation of κ and VFR

Here we present κ and VFR in direct relationship to each other which might help to assess the ongoing chemical processes and see the ranges of them. The trend of the volatility and the hygroscopicity evolution is similar during the O_3 mediated condensation and the OH mediated ripening, but shows the opposite trend after OH oxidation is initiated. Thus scatter plots of these two parameters are only useful for selected periods. Figure 8A shows for all available ozonolysis experiments (14 in total) the correlation of κ and VFR. The correlation is fair ($R^2 = 0.80$) and the observed scatter is attributed to different experimental conditions and periods. The correlation is governed by the chemistry during the O_3 mediated condensation where the strongest changes in κ and VFR are observed (see Sect. 3.2).

The correlation of κ and VFR in Fig. 8B allows a closer look at the temporal evolution during OH mediated condensation and ripening and the effect of "lights on" in four dark OH (TME) experiments (No. 11-14, see Table 2). Generally, the dark OH exposure experiments show a positive correlation between κ and VFR for about the first 10 h. Afterwards only the VFR increases further. Only an enhanced oxidation rate by turning on the lights producing more OH radicals increases VFR and κ even more (up to $\kappa = 0.2$). It should be cautioned here that the opposing trends of VFR and κ during the OH mediated condensing phase are buried in the scatter plot.

ACPD
11, 7423–7467, 2011

3.4.1 Maximum hygroscopicity and minimum volatility with addition of UV light

In one experiment we removed the UV-filters from the xenon lamps in the chamber. The combination of OH production with TME and ozone photolysis with unfiltered UV light results in a higher hygroscopicity (experiment No. 15, not shown in Fig. 8b). The highest hygroscopicity (κ = ~0.21) and lowest volatility (highest VFR = ~0.82 at 70 °C) of all experiments were reached in this experiment after only 4 h of OH aging (see Table 2). The experiment with second highest κ and VFR was the one with dark OH and (normal, see Sect. 2.1) lights on (No. 13). However, this was a long experiment with high O_3 concentration and we cannot decouple the effects. We conclude that both the additional OH (e.g. TME + lights) and enough time are important for aging.

3.5 Ripening and size dependence

In the following we present results from the second part of the experiments where OH mediated ripening was investigated. In addition we discuss the κ and VFR dependence on the particle's diameter. Figure 9 shows two different types of low concentration AP experiments: HONO photolysis (green traces) and dark OH (TME) experiment (yellow traces) with additional lights on (No. 5 and 14, see Table 2). The periods with lights on are indicated by arrows. In experiment No. 5 (green) the lights were the only OH source, in experiment No. 14 the lights were turned on and off in addition to the dark OH (TME) source. Organic aerosol mass, atomic O:C ratio (panel A and D) from the AMS and VFR as well as κ (panel B and C) are plotted against physical time after OH injection started. Dry diameters (D_0) are presented in different symbols.

All TDMA data are size-specific and the size dependence of the measured hygroscopicity and volatility has not been discussed so far. In experiment No. 14 the smaller particles tend to have a higher κ and lower VFR (higher volatility); this is not observed in experiment No. 5. The variation in κ between different D_0 is typically less than ± 0.01 (within uncertainty), in extreme cases up to 0.03, when comparing D_0 = 50 nm and D_0 = 150 nm. Usually several D_0, not too different from each other, are selected in the

ACPD
11, 7423–7467, 2011

TDMA to ensure a consistent measurement. Using the volatility data from the V-TDMA for experiment No. 14 from 6–9 h after the OH exposure as input for an evaporation model (Riipinen et al., 2010) showed a positive size dependence in the diameter range 100–150 nm – due to different evaporation kinetics of particles with different diameters. For this calculation, we approximated the SOA with a single component aerosol with saturation concentration of 1.2 $\mu g/m^3$ and a mass accommodation coefficient of unity, chosen to produce consistent results with the measured VFR at 100 nm. The SOA was assumed otherwise to have similar properties as the theoretical AP SOA modeled in Riipinen et al. (2010). Although this is a rough approximation, we believe it to be sufficient for this purpose of simply demonstrating the size-dependence of the evaporation kinetics. The size dependence predicted by the model is a bit stronger (VFR ranging from 0.71 to 0.83 with diameters ranging from 100 to 150 nm) than the one observed in our measurements (VFR from 0.71 to 0.75). The discrepancy in VFR between different D_0 sizes can thus probably be explained by simply kinetic effects rather than different volatilities of the particles with different sizes or measurement uncertainties or artifacts.

The two experiments No. 5 and 14 in Fig. 9 also illustrate well the interplay between OH mediated ripening and OH mediated condensation on VFR. The start of OH aging at time 0 resulted in an abrupt decrease in VFR (Fig. 9b) while SOA mass increased (OH mediated condensation phase) as already discussed above. When lights were turned off, the VFR increased by ripening (experiment No. 5) until lights were turned on again. The VFR then stayed constant while again SOA mass slightly increased. This is an indication that more of less volatile compounds are condensing compensating the ripening effect. In case of the TME experiment (No. 14) turning lights on enhances the OH exposure and more SOA mass is produced. Thus, VFR stays constant. This may indicate again that ripening is compensated by the condensation of low volatility compounds. When lights are turned off after 4.6 h VFR starts to increase. The ripening effect seems to be stronger than further condensation indicated by the slow SOA mass increase. Another lights on phase after 6.6 h does not change the ripening trend. This is also not expected as this time there was not much additional condensation observed.

ACPD
11, 7423–7467, 2011

The effects on κ are less pronounced. In general κ (panel C) increased with OH exposure while without OH, when lights were off (experiment No. 5, 2–4 h) κ slightly decreased.

4 Summary and conclusions

After careful construction, validation and characterization of a new V/H-TDMA we measured SOA during 15 different aging experiments with 10–40 ppb α-pinene within the MUCHACHAS campaign in the PSI smog chamber. The retrieved parameters VFR and κ for volatility and hygroscopicity are sensitive indicators of even small changes in the SOA properties. We assume that the observed changes of physical properties are caused by chemical changes as a result of functionalization, oligomerization or fragmentation. Two periods (condensation and ripening) were discerned for each reaction period (ozonolysis and OH exposure), as seen in Figs. 3 and 6. We introduced for these the terms O_3 mediated condensation and O_3 mediated ripening during ozonolysis and OH mediated condensation and OH mediated ripening during OH exposure. The first phase (O_3 mediated condensation) forms most of the SOA mass.

The original intent of these experiments was to observe changes in SOA physical properties (including total amounts) induced by exposure to OH radicals. Consistent with our hypotheses, we did observe significant changes in both SOA levels and volatility following exposure to OH. However, we also observed a sometimes slow, but steady evolution in both hygroscopicity and volatility in most experiments, which appears to be independent of exposure to OH. We hypothesize that this ripening is caused by relatively slow transformations of the condensed phase (this can include evaporation, oxidation, condensation cycles) which do not influence the SOA mass concentrations but do influence intensive physical and chemical properties (such as VFR, κ, O:C). Both of these phenomena appear to be significant and will require further attention.

Overall the particles' volatility decreases throughout the experiment. The VFR at 70 °C increases from about 0.5 up to 0.82 (after 4 h of aging) and 0.95 (after 20 h of

ACPD
11, 7423–7467, 2011

aging, Fig. 8). The hygroscopicity parameter κ ranges from 0.07 to 0.12 (GF from 1.28 to 1.40 at 95% RH) after the ozonolysis and increases significantly after OH exposure to κ 0.10–0.21 (GF 1.39–1.61) strongly dependent on the experiment and its conditions (Table 2). Production of new SOA seems to be the main driving force for the changes rather than aging of old SOA upon OH exposure. The κ range agrees well with the findings from other hygroscopicity studies for AP SOA (Petters and Kreidenweis, 2007; Duplissy et al., 2008). In agreement with Duplissy et al. (2008) κ values are lower for high AP experiments compared to the low AP concentration ones. These low κ values are explained with the partitioning of more volatile, less oxygenated compounds towards the particle phase at higher AP concentrations. The measured properties of our chamber SOA evolve almost continuously during aging, which is in contrast to other studies (Qi et al., 2010). They observed clearly lower hygroscopic GFs (at comparable RH) and slightly lower VFR at 100 °C (compare thermogram Fig. 4), probably due to different experimental conditions like low RH or less radiation intensity in their chamber.

The SOA is formed from the ozonolysis of the C=C double bond in α-pinene. Since O_3 does not react at other sites we expect that the first-generation oxidation products do not change during the ozonolysis reaction. The young aerosol seems to be fairly volatile with a VFR around 0.55-0.60, which then steadily increases. This indicates that reactions in the particles lead to less volatile compounds (oligomerization) as there are no second generation oxidation reactions in the gas phase yet. Heterogeneous reactions of O_3 on the surface of aerosols can be excluded as a higher O_3 concentration does not lead to a steeper increase in VFR (Figs. 5 and A). The low hygroscopicity in the beginning of the ozonolysis is consistent with a volatile, not strongly oxidized composition. The O:C ratio was measured to be 0.4–0.5 staying more or less constant or even slightly decreasing throughout the ozonolysis. With increasing SOA mass smaller compounds can partition into the aerosol leading to an increase in κ while oligomerization during the ripening phase would tend to decrease κ. When these aerosols are then exposed to OH the first generation volatile and semi-volatile products are further oxidized leading to further condensation onto the existing aerosol. This leads to

ACPD
11, 7423–7467, 2011

a sudden increase in volatility (decrease in VFR). Based on a simple two-compound model we estimate that this new SOA forming compounds are highly volatile (VFR <0.25 at 70 °C). During this OH mediated condensation phase both the hygroscopicity and the O:C ratio increase. All this indicates that fairly volatile, small and highly oxidized compounds, which are produced by functionalization and fragmentation of first generation products, are condensing during this phase. After the strong drop VFR increases again, indicating another ripening phase. Because there is still some more material condensing both of these two processes influence VFR and κ. As shown in Fig. 9 (see Sect. 3.5) condensation can be shut off by turning lights off (i.e., reducing the OH concentration), while the ripening (experiment No. 5) continues, resulting in an increasing VFR, but slightly decreasing κ and O:C ratio. We assume that this is due to oligomerization. In contrast, κ and the O:C ratio are more or less constant during the OH mediated ripening process for most experiments. We hypothesize that in this case the ongoing condensation is partly (VFR) or completely (κ and O:C) offsetting this effect.

There were no significant differences between dark OH (induced by tetramethylethylene, TME) and light OH (induced by HONO) aging found, and also high and low NO_x conditions had virtually no influence on the physical properties. Several parameters including AP, O_3 and OH concentration, SOA mass, organic aerosol atomic O:C ratio were analyzed with respect to their influence on the volatility and hygroscopicity. The combination of the physical properties volatility and hygroscopicity is a highly suitable approach to access the complex chemical processes during formation and aging of SOA. Future comprehensive studies should also include sophisticated chemical analysis of specific compounds in the aerosol phase combined with more trace gas measurements to be able to describe the ongoing processes in more detail.

ACPD
11, 7423–7467, 2011

Appendix A

The ozonolysis part in Sect. 3.2 analyzes the ongoing condensation and ripening processes. Figure A shows similar data as in Fig. 5 with the same symbols but on the chemical axis with O_3 exposure (in h ppb). This leads to a stretching or compressing of the data. Fig. 5 shows mainly a mix of concentration and time effects. Here we see (Fig. A) the O_3 dependence of VFR and κ which is mainly independent of the aerosol mass. The O_3 dose determines the starting point for the following OH reactions. The high O_3 concentration cases show lower κ, and higher O_3 concentration makes more volatile mass (lower VFR). κ and VFR increase mainly during the O_3 mediated condensation and are rather constant later (especially κ).

Acknowledgements. The authors thank René Richter and Günther Wehrle for the great support and work on the V/H-TDMA instrument and various smog chamber issues. This work was supported by the IMBALANCE project of the Competence Center Environment and Sustainability of the ETH Domain (CCES), as well as the Swiss National Science Foundation. PFD is grateful for postdoctoral research support from the US-NSF (IRFP #0701013).

References

Aiken, A. C., DeCarlo, P. F., and Jimenez, J. L.: Elemental analysis of organic species with electron ionization high-resolution mass spectrometry, Anal. Chem., 79, 8350–8358, doi:10.1021/ac071150w, 2007. 7429

Aiken, A. C., Decarlo, P. F., Kroll, J. H., Worsnop, D. R., Huffman, J. A., Docherty, K. S., Ulbrich, I. M., Mohr, C., Kimmel, J. R., Sueper, D., Sun, Y., Zhang, Q., Trimborn, A., Northway, M., Ziemann, P. J., Canagaratna, M. R., Onasch, T. B., Alfarra, M. R., Prevot, A. S. H., Dommen, J., Duplissy, J., Metzger, A., Baltensperger, U., and Jimenez, J. L.: O/C and OM/OC ratios of primary, secondary, and ambient organic aerosols with high-resolution time-of-flight aerosol mass spectrometry, Environ. Sci. Technol., 42, 4478–4485, doi:10.1021/es703009q, 2008. 7429

Alfarra, M. R., Paulsen, D., Gysel, M., Garforth, A. A., Dommen, J., Prevot, A. S. H., Worsnop, D. R., Baltensperger, U., and Coe, H.: A mass spectrometric study of secondary organic

ACPD

11, 7423–7467, 2011

aerosols formed from the photooxidation of anthropogenic and biogenic precursors in a reaction chamber, Atmos. Chem. Phys., 6, 5279–5293, doi:10.5194/acp-6-5279-2006, 2006. 7428

An, W. J., Pathak, R. K., Lee, B. H., and Pandis, S. N.: Aerosol volatility measurement using an improved thermodenuder: Application to secondary organic aerosol, J. Aerosol Sci., 38, 305–314, 2007. 7431, 7433, 7437, 7438

Baltensperger, U., Kalberer, M., Dommen, J., Paulsen, D., Alfarra, M. R., Coe, H., Fisseha, R., Gascho, A., Gysel, M., Nyeki, S., Sax, M., Steinbacher, M., Prevot, A. S. H., Sjogren, S., Weingartner, E., and Zenobi, R.: Secondary organic aerosols from anthropogenic and biogenic precursors, Faraday Discuss., 130, 265–278, 2005. 7426, 7437, 7438

Burtscher, H., Baltensperger, U., Bukowiecki, N., Cohn, P., Huglin, C., Mohr, M., Matter, U., Nyeki, S., Schmatloch, V., Streit, N., and Weingartner, E.: Separation of volatile and non-volatile aerosol fractions by thermodesorption: instrumental development and applications, J. Aerosol Sci., 32, 427–442, 2001. 7431

Chang, R. Y. W., Slowik, J. G., Shantz, N. C., Vlasenko, A., Liggio, J., Sjostedt, S. J., Leaitch, W. R., and Abbatt, J. P. D.: The hygroscopicity parameter (kappa) of ambient organic aerosol at a field site subject to biogenic and anthropogenic influences: relationship to degree of aerosol oxidation, Atmos. Chem. Phys., 10, 5047–5064, doi:10.5194/acp-10-5047-2010, 2010. 7426

Choi, M. Y. and Chan, C. K.: The effects of organic species on the hygroscopic behaviors of inorganic aerosols, Environ. Sci. Technol., 36, 2422–2428, doi:10.1021/es0113293, 2002. 7441

DeCarlo, P. F., Kimmel, J. R., Trimborn, A., Northway, M. J., Jayne, J. T., Aiken, A. C., Gonin, M., Fuhrer, K., Horvath, T., Docherty, K. S., Worsnop, D. R., and Jimenez, J. L.: Field-deployable, high-resolution, time-of-flight aerosol mass spectrometer, Anal. Chem., 78, 8281–8289, doi:10.1021/ac061249n, 2006. 7428

Donahue, N. M., Robinson, A. L., Stanier, C. O., and Pandis, S. N.: Coupled partitioning, dilution, and chemical aging of semivolatile organics, Environ. Sci. Technol., 40, 2635-2643, doi:10.1021/esO52297c, 2006. 7425

Duplissy, J., Gysel, M., Alfarra, M. R., Dommen, J., Metzger, A., Prevot, A. S. H., Weingartner, E., Laaksonen, A., Raatikainen, T., Good, N., Turner, S. F., McFiggans, G., and Baltensperger, U.: Cloud forming potential of secondary organic aerosol under near atmospheric conditions, Geophys. Res. Lett., 35(5), L03818, doi:10.1029/2007GL031075, 2008. 7426, 7429, 7439, 7447

ACPD

11, 7423–7467, 2011

Duplissy, J., Gysel, M., Sjogren, S., Meyer, N., Good, N., Kammermann, L., Michaud, V., Weigel, R., Martins dos Santos, S., Gruening, C., Villani, P., Laj, P., Sellegri, K., Metzger, A., McFiggans, G. B., Wehrle, G., Richter, R., Dommen, J., Ristovski, Z., Baltensperger, U., and Weingartner, E.: Intercomparison study of six HTDMAs: results and recommendations, Atmos. Meas. Tech., 2, 363–378, doi:10.5194/amt-2-363-2009, 2009. 7429

Duplissy, J., DeCarlo, P. F., Dommen, J., Alfarra, M. R., Metzger, A., Barmpadimos, I., Prevot, A. S. H., Weingartner, E., Tritscher, T., Gysel, M., Aiken, A. C., Jimenez, J. L., Canagaratna, M. R., Worsnop, D. R., Collins, D. R., Tomlinson, J., and Baltensperger, U.: Relating hygroscopicity and composition of organic aerosol particulate matter, Atmos. Chem. Phys.,11, 1155–1165, doi:10.5194/acp-11-1155-2011, 2011. 7426, 7429

Epstein, S. A., and Donahue, N. M.: The kinetics of tetramethylethene ozonolysis: Decomposition of the primary ozonide and subsequent product formation in the condensed phase, J. Phys. Chem. A, 112, 13535–13541, doi:10.1021/jp807682y, 2008. 7435

Gysel, M., Crosier, J., Topping, D. O., Whitehead, J. D., Bower, K. N., Cubison, M. J., Williams, P. I., Flynn, M. J., McFiggans, G. B., and Coe, H.: Closure study between chemical composition and hygroscopic growth of aerosol particles during TORCH2, Atmos. Chem. Phys., 7, 6131–6144, doi:10.5194/acp-7-6131-2007, 2007. 7441

Gysel, M., McFiggans, G. B., and Coe, H.: Inversion of tandem differential mobility analyser (TDMA) measurements, J. Aerosol Sci., 40, 134–151, doi:10.1016/j.jaerosci.2008.07.013, 2009. 7431

Hallquist, M., Wenger, J. C., Baltensperger, U., Rudich, Y., Simpson, D., Claeys, M., Dommen, J., Donahue, N. M., George, C., Goldstein, A. H., Hamilton, J. F., Herrmann, H., Hoffmann, T., Iinuma, Y., Jang, M., Jenkin, M. E., Jimenez, J. L., Kiendler-Scharr, A., Maenhaut, W., McFiggans, G., Mentel, T. F., Monod, A., Prevot, A. S. H., Seinfeld, J. H., Surratt, J. D., Szmigielski, R., and Wildt, J.: The formation, properties and impact of secondary organic aerosol: current and emerging issues, Atmos. Chem. Phys., 9, 5155–5236, doi:10.5194/acp-9-5155-2009, 2009. 7425, 7427

Hodzic, A., Jimenez, J. L., Madronich, S., Canagaratna, M. R., DeCarlo, P. F., Kleinman, L., and Fast, J.: Potential contribution of semi-volatile and intermediate volatility primary organic compounds to secondary organic aerosol in the Mexico City region, Atmos. Chem. Phys., 10, 5491–5514, doi:10.5194/acp-10-5491-2010, 2010. 7425

Huffman, J. A., Ziemann, P. J., Jayne, J. T., Worsnop, D. R., and Jimenez, J. L.: Development and characterization of a fast-stepping/scanning thermodenuder for

ACPD
11, 7423–7467, 2011

chemically-resolved aerosol volatility measurements, Aerosol Sci. Technol., 42, 395–407, doi:10.1080/02786820802104981, 2008. 7433, 7437

Huffman, J. A., Docherty, K. S., Mohr, C., Cubison, M. J., Ulbrich, I. M., Ziemann, P. J., Onasch, T. B., and Jimenez, J. L.: Chemically-resolved volatility measurements of organic aerosol from different sources, Environ. Sci. Technol., 43, 5351–5357, doi:10.1021/es803539d, 2009. 7437

Jimenez, J. L., Canagaratna, M. R., Donahue, N. M., Prevot, A. S. H., Zhang, Q., Kroll, J. H., DeCarlo, P. F., Allan, J. D., Coe, H., Ng, N. L., Aiken, A. C., Docherty, K. S., Ulbrich, I. M., Grieshop, A. P., Robinson, A. L., Duplissy, J., Smith, J. D., Wilson, K. R., Lanz, V. A., Hueglin, C., Sun, Y. L., Tian, J., Laaksonen, A., Raatikainen, T., Rautiainen, J., Vaattovaara, P., Ehn, M., Kulmala, M., Tomlinson, J. M., Collins, D. R., Cubison, M. J., Dunlea, E. J., Huffman, J. A., Onasch, T. B., Alfarra, M. R., Williams, P. I., Bower, K., Kondo, Y., Schneider, J., Drewnick, F., Borrmann, S., Weimer, S., Demerjian, K., Salcedo, D., Cottrell, L., Griffin, R., Takami, A., Miyoshi, T., Hatakeyama, S., Shimono, A., Sun, J. Y., Zhang, Y. M., Dzepina, K., Kimmel, J. R., Sueper, D., Jayne, J. T., Herndon, S. C., Trimborn, A. M., Williams, L. R., Wood, E. C., Middlebrook, A. M., Kolb, C. E., Baltensperger, U., and Worsnop, D. R.: Evolution of organic aerosols in the atmosphere, Science, 326, 1525–1529, doi:10.1126/science.1180353, 2009. 7425, 7426

Jonsson, A. M., Hallquist, M., and Saathoff, H.: Volatility of secondary organic aerosols from the ozone initiated oxidation of alpha-pinene and limonene, J. Aerosol Sci., 38, 843–852, 2007. 7430, 7437, 7438

Juranyi, Z., Gysel, M., Duplissy, J., Weingartner, E., Tritscher, T., Dommen, J., Henning, S., Ziese, M., Kiselev, A., Stratmann, F., George, I., and Baltensperger, U.: Influence of gas-to-particle partitioning on the hygroscopic and droplet activation behaviour of alpha-pinene secondary organic aerosol, Phys. Chem. Chem. Phys., 11, 8091–8097, doi:10.1039/b904162a, 2009. 7426

Kalberer, M., Paulsen, D., Sax, M., Steinbacher, M., Dommen, J., Prevot, A. S. H., Fisseha, R., Weingartner, E., Frankevich, V., Zenobi, R., and Baltensperger, U.: Identification of polymers as major components of atmospheric organic aerosols, Science, 303, 1659–1662, 2004. 7426

Lindinger, W., Hansel, A., and Jordan, A.: On-line monitoring of volatile organic compounds at pptv levels by means of proton-transfer-reaction mass spectrometry (PTR-MS) – Medical applications, food control and environmental research, Int. J. Mass Spectrom., 173, 191–241,

ACPD
11, 7423–7467, 2011

1998. 7429
Lohmann, U., and Feichter, J.: Global indirect aerosol effects: a review, Atmos. Chem. Phys., 5, 715–737, doi:10.5194/acp-5-715-2005, 2005. 7426
Massoli, P., Lambe, A. T., Ahern, A. T., Williams, L. R., Ehn, M., Mikkila, J., Canagaratna, M. R., Brune, W. H., Onasch, T. B., Jayne, J. T., Petaja, T., Kulmala, M., Laaksonen, A., Kolb, C. E., Davidovits, P., and Worsnop, D. R.: Relationship between aerosol oxidation level and hygroscopic properties of laboratory generated secondary organic aerosol (SOA) particles, Geophys. Res. Lett., 37(5), L24801, doi:10.1029/2010gl045258, 2010. 7426
Modini, R. L., Harris, B., and Ristovski, Z. D.: The organic fraction of bubble-generated, accumulation mode sea spray aerosol (SSA), Atmos. Chem. Phys., 10, 2867–2877, doi:10.5194/acp-10-2867-2010, 2010. 7432
Moore, R. H., and Raymond, T. M.: HTDMA analysis of multicomponent dicarboxylic acid aerosols with comparison to UNIFAC and ZSR, J. Geophys. Res.-Atmos., 113, 15, D04206, doi:10.1029/2007jd008660, 2008. 7441
Pankow, J. F.: An absorption-model of gas-particle partitioning involved in the formation of secondary organic aerosol, Atmos. Environ., 28, 189–193, 1994a. 7425
Pankow, J. F.: An absorption-model of gas-particle partitioning of organic-compounds in the atmosphere, Atmos. Environ., 28, 185–188, 1994b. 7425
Park, D., Kim, S., Choi, N. K., and Hwang, J.: Development and performance test of a thermo-denuder for separation of volatile matter from submicron aerosol particles, J. Aerosol Sci., 39, 1099–1108, doi:10.1016/j.jaerosei.2008.07.002, 2008. 7433
Pathak, R. K., Stanier, C. O., Donahue, N. M., and Pandis, S. N.: Ozonolysis of alpha-pinene at atmospherically relevant concentrations: Temperature dependence of aerosol mass fractions (yields), J. Geophys. Res.-Atmos., 112(8), D03201 doi:10.1029/2006jd007436, 2007. 7428
Paulsen, D., Dommen, J., Kalberer, M., Prevot, A. S. H., Richter, R., Sax, M., Steinbacher, M., Weingartner, E., and Baltensperger, U.: Secondary organic aerosol formation by irradiation of 1,3,5-trimethylbenzene-NO_x-H_2O in a new reaction chamber for atmospheric chemistry and physics, Environ. Sci. Technol., 39, 2668–2678, 2005. 7428, 7430, 7437, 7438
Petters, M. D. and Kreidenweis, S. M.: A single parameter representation of hygroscopic growth and cloud condensation nucleus activity, Atmos. Chem. Phys., 7, 1961–1971, doi:10.5194/acp-7-1961-2007, 2007. 7426, 7432, 7447
Petters, M. D., Kreidenweis, S. M., Snider, J. R., Koehler, K. A., Wang, Q., Prenni, A. J., and Demott, P. J.: Cloud droplet activation of polymerized organic aerosol, Tellus Ser. B-Chem.

ACPD
11, 7423–7467, 2011

Phys. Meteorol., 58, 196–205, doi:10.1111/j.1600-0889.2006.00181.x, 2006. 7427
Petters, M. D., Wex, H., Carrico, C. M., Hallbauer, E., Massling, A., McMeeking, G. R., Poulain, L., Wu, Z., Kreidenweis, S. M., and Stratmann, F.: Towards closing the gap between hygroscopic growth and activation for secondary organic aerosol – Part 2: Theoretical approaches, Atmos. Chem. Phys., 9, 3999–4009, doi:10.5194/acp-9-3999-2009, 2009. 7427
Prenni, A. J., Petters, M. D., Kreidenweis, S. M., DeMott, P. J., and Ziemann, P. J.: Cloud droplet activation of secondary organic aerosol, J. Geophys. Res.-Atmos., 112(12), D10223, doi:10.1029/2006JD007963, 2007. 7426
Qi, L., Nakao, S., Malloy, Q., Warren, B., and Cocker, D. R.: Can secondary organic aerosol formed in an atmospheric simulation chamber continuously age?, Atmos. Environ., 44, 2990–2996, doi:10.1016/j.atmosenv.2010.05.020, 2010. 7426, 7447
Rader, D. J., and McMurry, P. H.: Application of the tandem differential mobility analyzer to studies of droplet growth or evaporation, J. Aerosol Sci., 17, 771–787, 1986. 7429
Reinhardt, A., Emmenegger, C., Gerrits, B., Panse, C., Dommen, J., Baltensperger, U., Zenobi, R., and Kalberer, M.: Ultrahigh mass resolution and accurate mass measurements as a tool to characterize oligomers in secondary organic aerosols, Anal. Chem., 79, 4074–4082, doi:10.1021/ac062425v, 2007. 7426
Riipinen, I., Pierce, J. R., Donahue, N. M., and Pandis, S. N.: Equilibration time scales of organic aerosol inside thermodenuders: Evaporation kinetics versus thermodynamics, Atmos. Environ., 44, 597–607, doi:10.1016/j.atmosenv.2009.11.022, 2010. 7433, 7438, 7445
Robinson, A. L., Donahue, N. M., Shrivastava, M. K., Weitkamp, E. A., Sage, A. M., Grieshop, A. P., Lane, T. E., Pierce, J. R., and Pandis, S. N.: Rethinking organic aerosols: Semivolatile emissions and photochemical aging, Science, 315, 1259–1262, doi:10.1126/science.1133061, 2007. 7425
Rudich, Y., Donahue, N. M., and Mentel, T. F.: Aging of organic aerosol: Bridging the gap between laboratory and field studies, Annu. Rev. Phys. Chem., 58, 321–352, 2007. 7425
Scheibel, H. G., and Porstendoerfer, J.: Generation of monodisperse Ag- and NaCl-aerosol with particle diameters between 2 nm and 300 nm, J. Aerosol Sci., 14, 113–126, 1983. 7432
Sjogren, S., Gysel, M., Weingartner, E., Alfarra, M. R., Duplissy, J., Cozic, J., Crosier, J., Coe, H., and Baltensperger, U.: Hygroscopicity of the submicrometer aerosol at the high-alpine site Jungfraujoch, 3580 m a.s.l., Switzerland, Atmos. Chem. Phys., 8, 5715–5729, doi:10.5194/acp-8-5715-2008, 2008. 7441
Stokes, R. H., and Robinson, R. A.: Interactions in aqueous nonelectrolyte solutions. I. Solute-

ACPD
11, 7423–7467, 2011

solvent equilibria, J. Phys. Chem., 70, 2126–2131, 1966. 7441
Swietlicki, E., Hansson, H. C., Hameri, K., Svenningsson, B., Massling, A., McFiggans, G., McMurry, P. H., Petaja, T., Tunved, P., Gysel, M., Topping, D., Weingartner, E., Baltensperger, U., Rissler, J., Wiedensohler, A., and Kulmala, M.: Hygroscopic properties of submicrometer atmospheric aerosol particles measured with H-TDMA instruments in various environments - a review, Tellus Ser. B-Chem. Phys. Meteorol., 60, 432–469, doi:10.1111/j.1600-0889.2008.00350.x, 2008. 7429
Taira, M., and Kanda, Y.: Continuous generation system for low-concentration gaseous nitrous-acid, Anal. Chem., 62, 630–633, 1990. 7435
Varutbangkul, V., Brechtel, F. J., Bahreini, R., Ng, N. L., Keywood, M. D., Kroll, J. H., Flagan, R. C., Seinfeld, J. H., Lee, A., and Goldstein, A. H.: Hygroscopicity of secondary organic aerosols formed by oxidation of cycloalkenes, monoterpenes, sesquiterpenes, and related compounds, Atmos. Chem. Phys., 6, 2367–2388, doi:10.5194/acp-6-2367-2006, 2006. 7426
Villani, P., Picard, D., Marchand, N., and Laj, P.: Design and validation of a 6-volatility tandem differential mobility analyzer (VTDMA), Aerosol Sci. Technol., 41, 898–906, 2007. 7430, 7433
Volkamer, R., Jimenez, J. L., San Martini, F., Dzepina, K., Zhang, Q., Salcedo, D., Molina, L. T., Worsnop, D. R., and Molina, M. J.: Secondary organic aerosol formation from anthropogenic air pollution: Rapid and higher than expected, Geophys. Res. Lett., 33(4), L17811, doi:10.1029/2006gl026899, 2006. 7425
Wehner, B., Philippin, S., and Wiedensohler, A.: Design and calibration of a thermodenuder with an improved heating unit to measure the size-dependent volatile fraction of aerosol particles, J. Aerosol Sci., 33, 1087–1093, 2002. 7431
Wu, Z. J., Poulain, L., Wehner, B., Wiedensohler, A., and Herrmann, H.: Characterization of the volatile fraction of laboratory-generated aerosol particles by thermodenuder-aerosol mass spectrometer coupling experiments, J. Aerosol Sci., 40, 603–612, doi:10.1016/j.jaerosci.2009.03.007, 2009. 7433

ACPD
11, 7423–7467, 2011

Table 1. The three main chemical processes and their expected influence on volatility and hygroscopicity, and on additional parameters: van't Hoff factor i_s; the ratio of density to molar weight of solute, ρ_s/M_s. Symbols represent: + expected to increase, – expected to decrease, ~ only minor change expected. For hygroscopicity (κ) see also Eq. (1).

	functionalization	oligomerization	fragmentation
volatility	–	–	+
VFR (volume fraction remaining)	+	+	–
i_s	+/~	~	~
ρ_s/M_s	~	–	+
hygroscopicity (κ)	+/~	–	+

ACPD
11, 7423–7467, 2011

Table 2. Overview for all smog chamber experiments during the MUCHACHAS campaign 2009 at PSI with detailed experiment conditions (AP and O_3 input) and results from the V/H-TDMA.

	exp. ID/No.	experiment type	exp. date	nominal AP input	nominal O_3 input	comments on the experiment	hygroscopic growth factor at RH of 95% and (κ value)			volume fraction remaining at temperature of 70 °C			comments on V/H-TDMA
			dd mm yyyy	[ppb]	[ppb]		before OH aging	2 h OH aging	4 h OH aging	before OH aging	2 h OH aging	4 h OH aging	
ozonolysis only	1	O_3 only	26 Jan 2009	40	500		1.32 (0.083)	–	–	0.71	–	–	thermogram
	2	O_3 only	18 Feb 2009	40	500	no AMS data	1.28 (0.069)	–	–	0.81	–	–	thermogram
ozonolysis and light OH, HONO photolysis	3	O_3 + HONO + light	16 Jan 2009	40	100+300	only 1st part used, H_2SO_4 during HONO	1.37 (0.096)	1.47 (0.133)	1.50 (0.139)	0.61	0.58	0.72	only ozonolysis part used; thermogram
	4	O_3 + HONO + light	21 Jan 2009	10	150+50		1.38 (0.113)	1.46 (0.138)	1.48 (0.141)	0.70	0.63	–	
	5	O_3 + HONO + light	11 Feb 2009	10	250+50	lights ON/OFF	1.35 (0.100)	1.42 (0.138)	1.42 (0.120)	0.68	0.64	0.70	
	6	O_3 + HONO + NO + light	19 Jan 2009	40	90+20		1.37 (0.097)	1.43 (0.116)	1.46 (0.131)	0.66	0.58	–	thermogram
	7	O_3 + HONO + NO + light	13 Feb 2009	40	150+100		1.31 (0.084)	1.39 (0.106)	1.39 (0.108)	0.65	0.59	0.61	
	8	O_3 + HONO + NO + light	23 Jan 2009	10	200		1.40 (0.115)	1.42 (0.123)	1.43 (0.128)	0.71	0.64	0.78	thermogram
	9	O_3 + light	14 Jan 2009	40	200	very short experiment	1.19* (0.084)	1.21* (0.094)	–	0.70	0.67	–	*H-TDMA at 90% RH; only thermogram
	10	O_3+light	6 Feb 2009	10	200	lights ON/OFF	1.40 (0.115)	1.46 (0.139)	1.49 (0.148)	0.72	0.69	0.74	
ozonolysis and dark OH, TME ozonolysis	11	O_3 + TME	28 Jan 2009	40	500+200	long exp.	1.29 (0.072)	1.36 (0.093)	1.39 (0.104)	0.56	0.57	0.60	thermogram
	12	O_3 + TME	23 Feb 2009	10	500	no AMS data	1.34 (0.106)	1.40 (0.129)	1.44 (0.145)	0.67	0.60–0.63	0.61–0.65	
	13	O_3 + TME + lights	2 Feb 2009	10	500+150 +150	long exp.; lights ON at end of exp.	1.34 (0.098)	1.41 (0.125)	1.44 (0.135)	0.65	0.62	–	thermogram
	14	O_3 + TME + lights	9 Feb 2009	10	500+150	lights ON/OFF	1.35 (0.094)	1.42 (0.137)	1.45 (0.139)	0.66	0.62–0.66	0.66	
	15	O_3 + TME + lights	25 Feb 2009	10	500	UV intensiv lights in addition to TME; no AMS data	1.31 (0.087)	1.35 (0.103)	1.61 (0.206)	0.63	0.62	0.82	(thermogram)

ACPD
11, 7423–7467, 2011

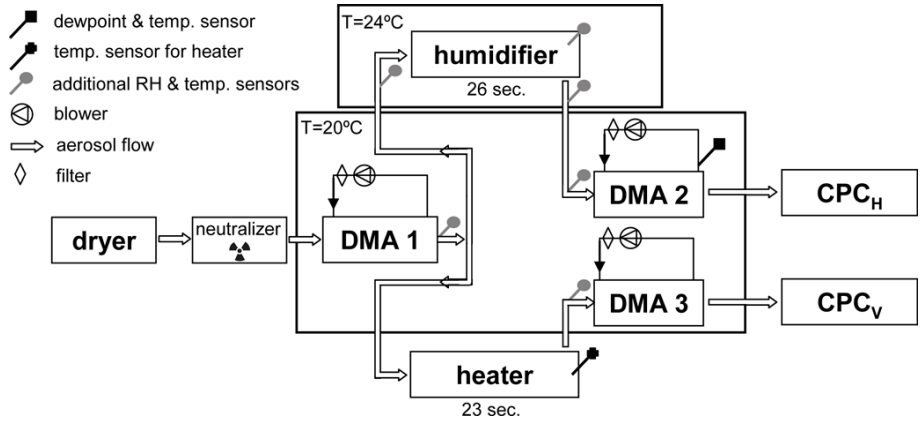

Fig. 1. Schematic of the combined volatility and hygroscopicity tandem differential mobility analyzer (V/H-TDMA) setup with the main instrument parts and sensors. The reference RH of the humidified branch is calculated from the dewpoint and temperature measured by a dew point mirror at the excess air outlet DMA2. The reference temperature for the V-branch is just before the outlet of the heater. The given residence times are measured between outlet of DMA1 and DMA2 or DMA3, respectively.

ACPD
11, 7423–7467, 2011

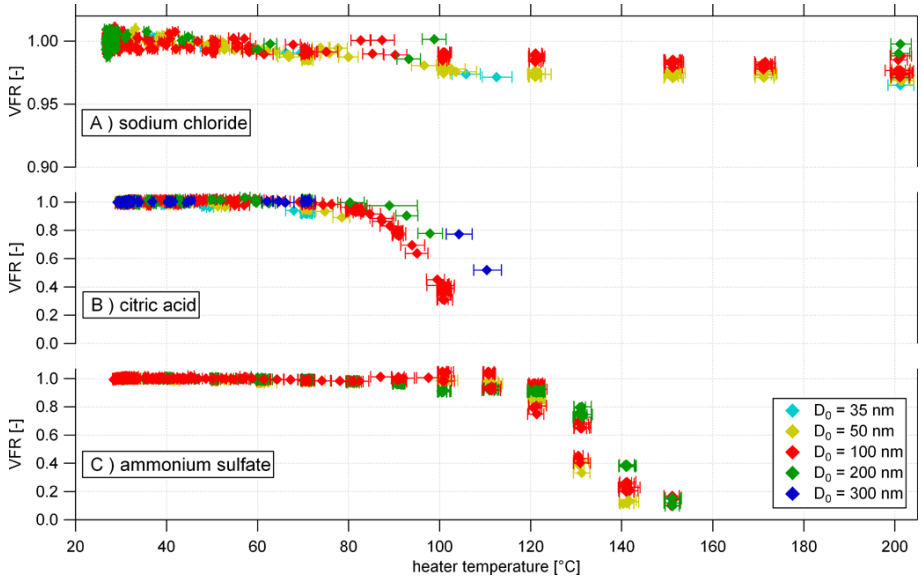

Fig. 2. Thermograms, normalized volume fraction remaining (VFR) plotted against the measured heater temperature, for sodium chloride (NaCl) (panel **A**), citric acid (panel **B**) and ammonium sulfate (AS) (panel **C**) as retrieved from the V-TDMA measurements. Different dry diameters (D_0) are distinguished by color and the error bars represent the minimal and maximal temperature during a scan.

ACPD
11, 7423–7467, 2011

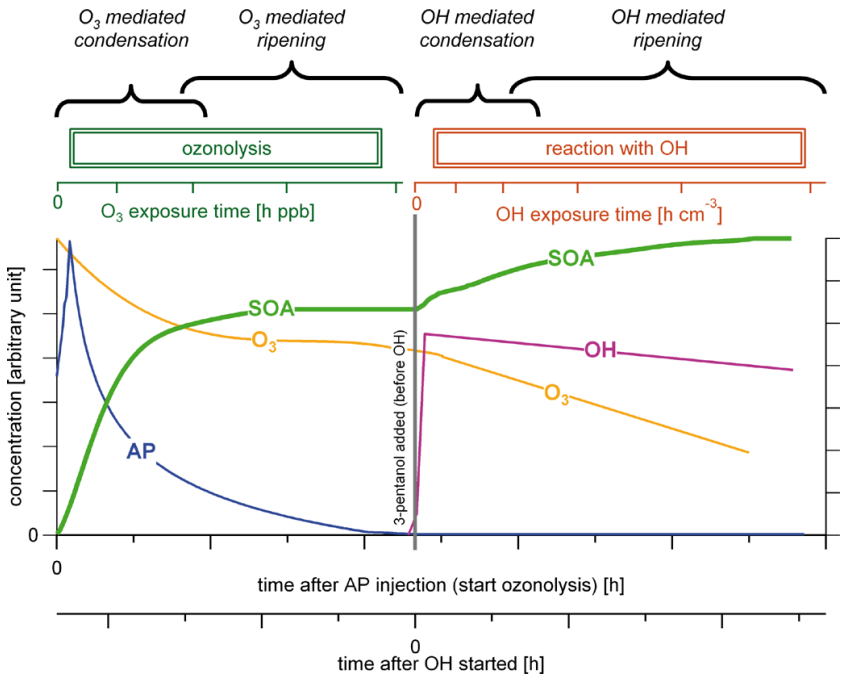

Fig. 3. Schematic of the main features of the smog chamber experiments during MUCHACHAS. Formation of secondary organic aerosol (SOA) mass (wall-loss corrected) from the volatile organic precursor α-pinene (AP) takes place during the first part in dark with ozone (O_3). The ozonolysis is followed by OH chemistry to age the SOA. The data can be plotted against several time axes in "physical time" as time after AP injection was started and time after the OH reaction started or against a chemical time clock as O_3 exposure time and OH exposure time. During ozonolysis and reaction with OH the four dominating mechanisms for four different phases of our experiments are indicated above the figure with curly braces: O_3 mediated condensation, O_3 mediated ripening, OH mediated condensation, and OH mediated ripening.

ACPD
11, 7423–7467, 2011

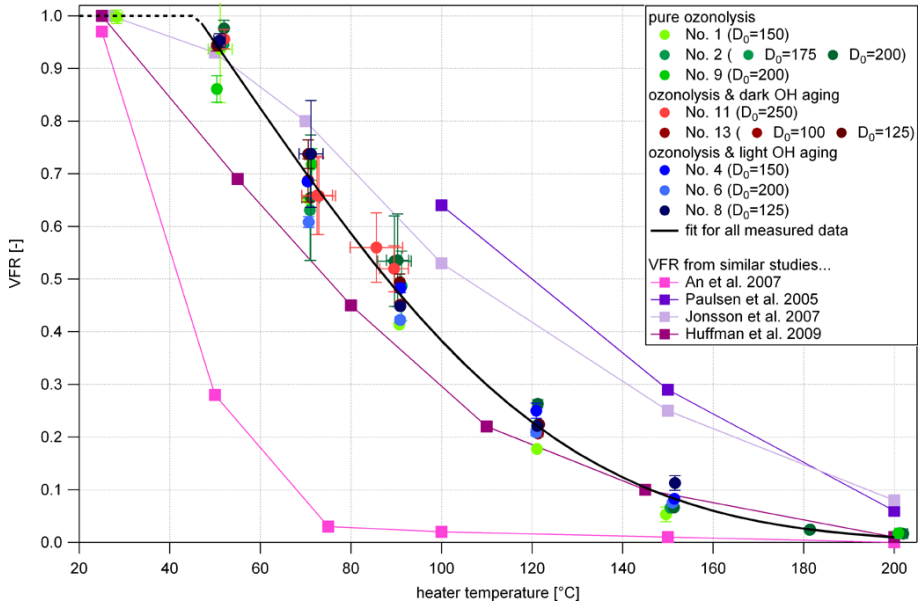

Fig. 4. Mean VFR (circles) measured for SOA from three different experiment types, distinguished with greenish, reddish and bluish color, at various heater temperatures with error bars representing the standard deviation of VFR and temperature of multiple measurements during the experiment. Literature data (squares) from similar SOA studies were added for comparison. The black solid line represents a fit though all measured data of this study.

ACPD
11, 7423–7467, 2011

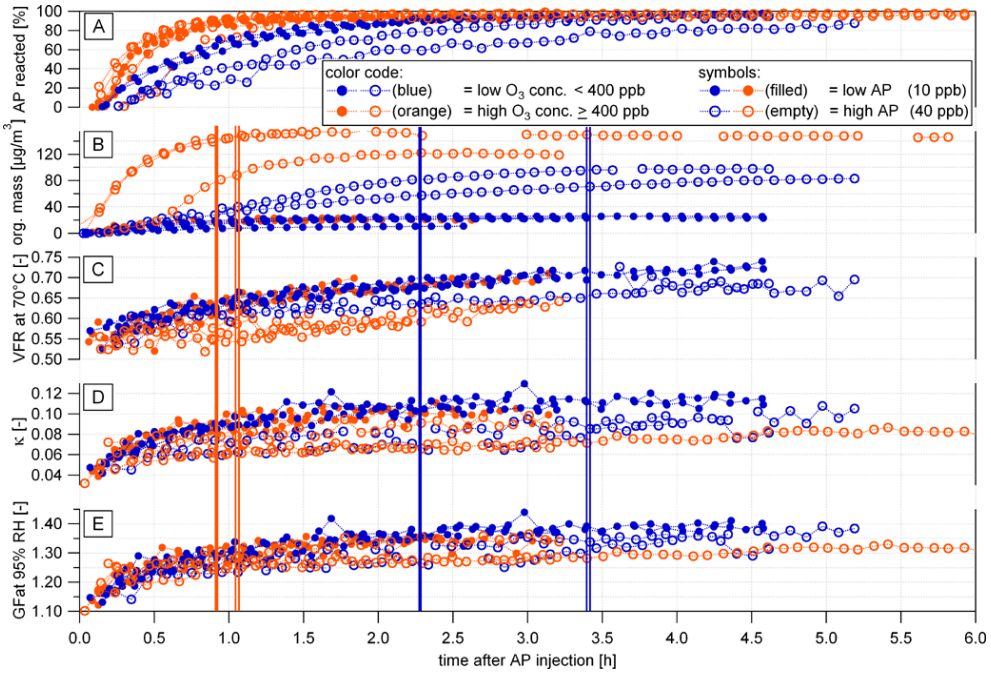

Fig. 5. All experiments of the ozonolysis part only. The color indicates the O_3 concentration, blue for low O_3 (<400 ppb) and orange for high O_3 (≥400 ppb). The filled symbols represent the low α-pinene (AP) (10 ppb) and open symbols the high AP (40 ppb) precursor concentration experiments. The relative fraction of AP reacted, wall-loss corrected SOA mass concentration (org. mass), volatility expressed as VFR at 70 °C, the hygroscopic parameter κ, and the GF at 95% RH (panel **A**–**E**) are plotted against the time after AP was injected into the smog chamber (physical time). The vertical lines indicate roughly the 90%-AP-reacted value for the four main experiment conditions: high/low AP (open/solid line, respectively), combined with high/low O_3 (orange/blue color, respectively).

ACPD
11, 7423–7467, 2011

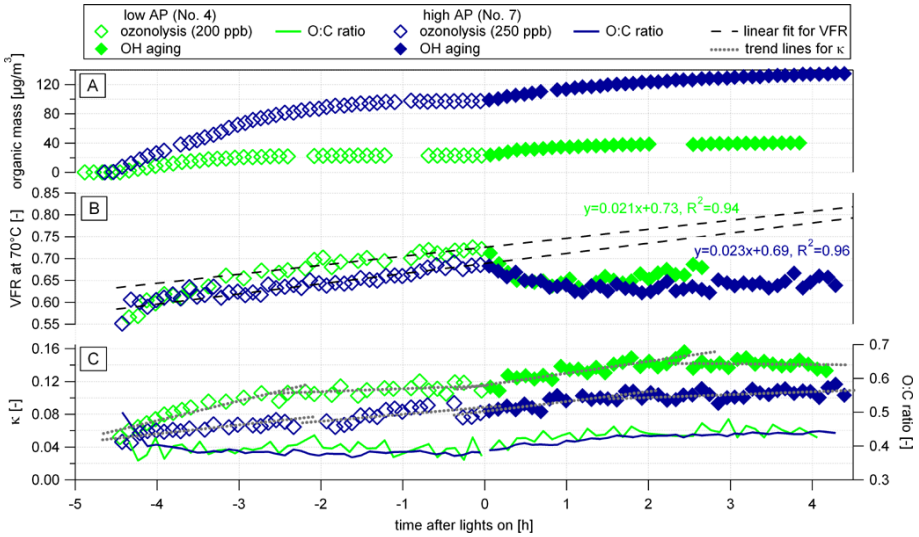

Fig. 6. Time series of two α-pinene (AP) ozonolysis experiments followed by reaction with OH from HONO photolysis. The two phases of the experiment, ozonolysis and reaction with OH, are distinguished by open and closed symbols, respectively, and green and blue color is used for the low (10 ppb) and high (40 ppb) AP precursor concentration experiment, respectively. Panel **(A)** shows the organic aerosol mass (wall-loss corrected), panel **(B)** the VFR at 70 °C and in panel **(C)** the hygroscopicity parameter κ (left axis) as well as the O:C ratio (right axis). The evolution of the VFR during O_3 mediated ripening (ca. from −3 to 0 h) was linearly fitted and extrapolated to indicate the trend expected without reaction with OH. The grey dotted lines shown in panel **(C)** help to guide the eye to see the changing trends of κ in the four periods of the experiment.

ACPD
11, 7423–7467, 2011

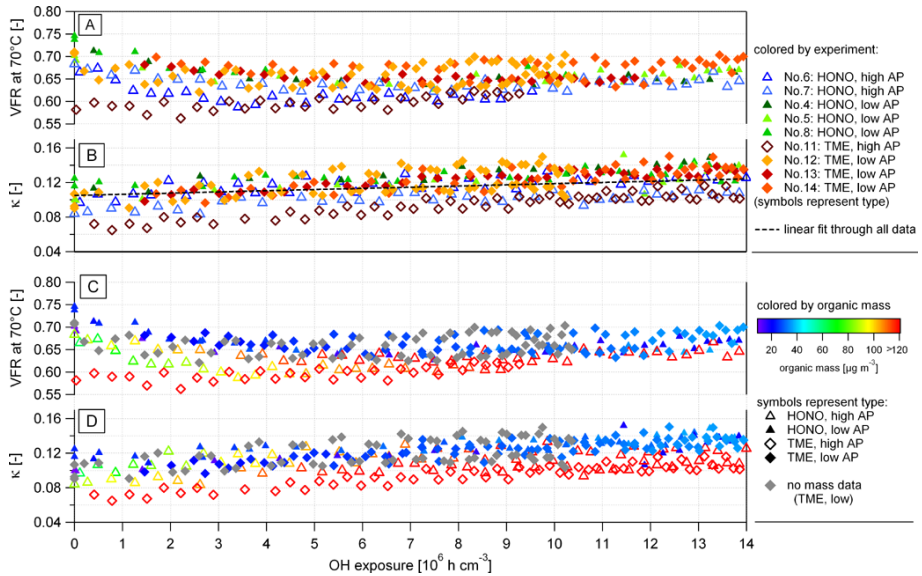

Fig. 7. Volatility, expressed as VFR at 70 °C, and hygroscopicity parameter κ plotted against the chemical clock OH exposure time shown for the reaction with OH part of the experiments only. The color code in panel **(A)** and **(B)** represents the individual experiments; while the symbols shape and filling indicate the experiment type and α-pinene (AP) input concentration, respectively. The filled symbols represent the low AP (10 ppb) and open symbols the high AP (40 ppb) precursor concentration experiments. Panel **(C)** and **(D)** show exactly the same data as panels **(A)** and **B**, now arranged in groups of experiment type and color coded by their wall-loss corrected organic aerosol mass (note that the red color ranges from 120 to max. 255 g/m^3).

ACPD
11, 7423–7467, 2011

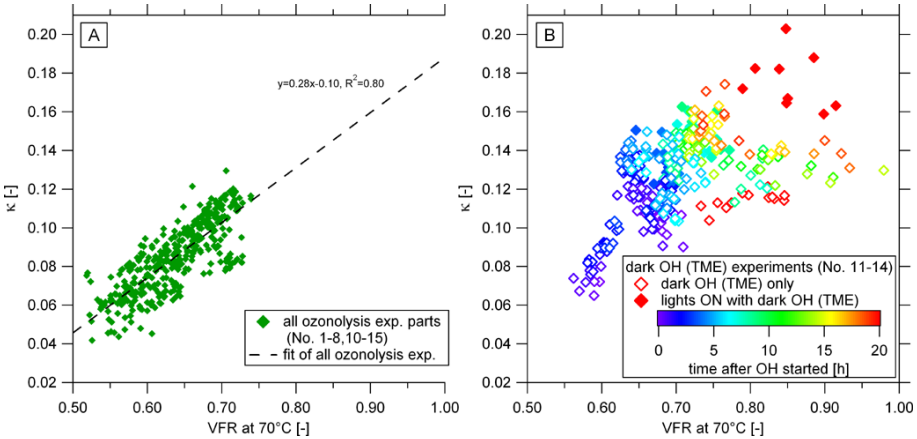

Fig. 8. Correlation of hygroscopicity parameter κ and VFR at 70 °C of α-pinene SOA shown in panel **(A)** for all available experiments during the ozonolysis part only. The same correlation is shown in panel **(B)** for experiments No. 11-14 during the reaction with OH from TME in absence of light (open symbols), sometimes with addition of lights (closed symbols). The data shown in panel **(B)** are color coded by time after OH started.

ACPD
11, 7423–7467, 2011

Volatility and hygroscopicity of aging SOA in a smog chamber

T. Tritscher et al.

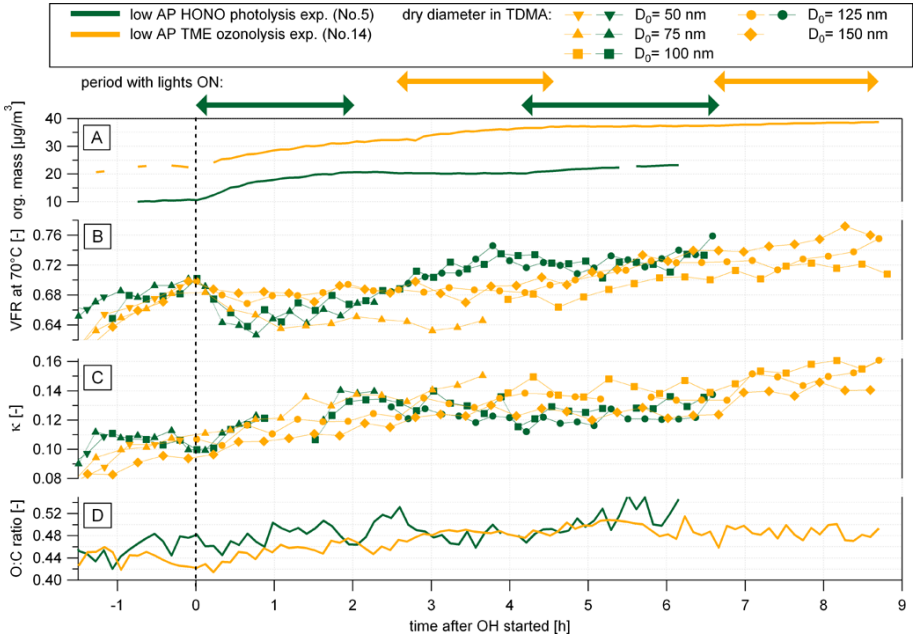

Fig. 9. Results from low concentration α-pinene experiments No. 5 (OH from HONO photolysis, green) and 14 (OH from TME, yellow) are plotted as time series of: **(A)** wall-loss corrected organic aerosol mass (org. mass), **(B)** volatility as VFR at 70 °C, **(C)** hygroscopicity parameter κ, and **(D)** O:C ratio. The lights were intermittently turned on and off during these two experiments. The double arrows above the figure indicate the periods with lights on. The symbols in panel **(B)** and **(C)** indicate the dry diameter (D_0) for the TDMA measurement and show the size dependence of volatility and hygroscopicity.

ACPD
11, 7423–7467, 2011

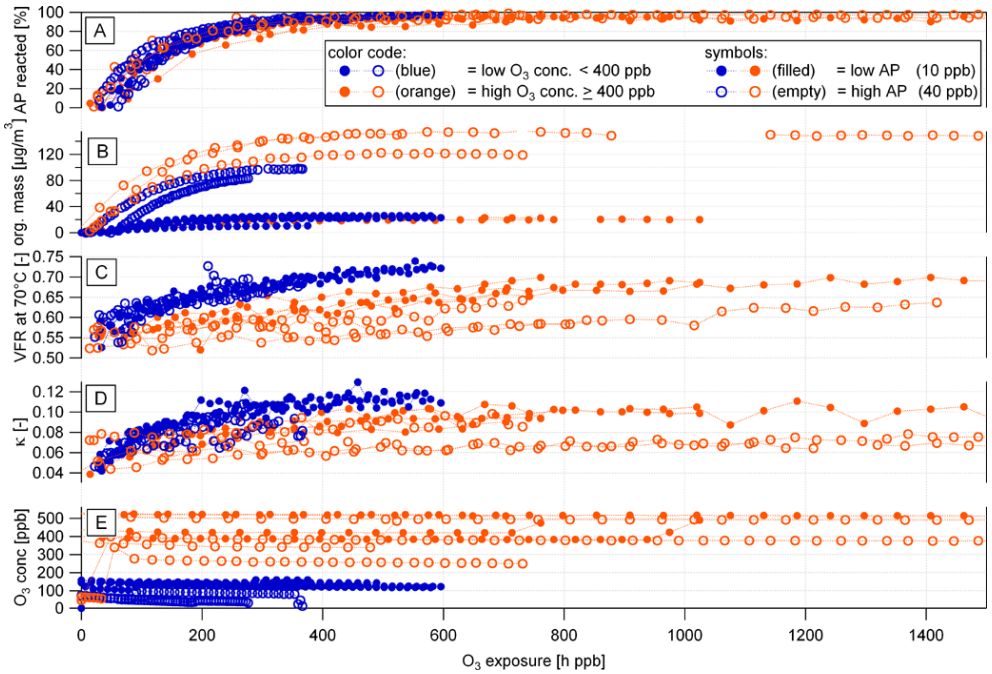

Fig. A1. The relative fraction α-pinene (AP) reacted, SOA mass (org. mass), volatility as VFR at 70 °C, hygroscopicity parameter κ, and the O_3 concentration (panel **A–E**) are plotted against the integrated O_3 exposure time (chemical time). The color indicates the O_3 concentration in blue for low O_3 (<400 ppb) and orange for high O_3 (≥400 ppb), respectively. The filled symbols represent low AP and open symbols the high AP precursor experiments (compare Fig. 5).

ACPD
11, 7423–7467, 2011